EUROPEAN ORGANIZATION FOR NUCLEAR RESEARCH

CERN-PPE/91-94
12 June 1991

Measurement of the Polarization of τ Leptons Produced in Z Decays

The ALEPH Collaboration

Abstract

The polarization of τ leptons produced in the reaction $e^+e^- \rightarrow \tau^+\tau^-$ at the Z resonance has been measured using the τ decay modes $e\nu_e\nu_\tau$, $\mu\nu_\mu\nu_\tau$, $\pi\nu_\tau$, $\rho\nu_\tau$, and $a_1\nu_\tau$. The mean value obtained is $P_\tau = -0.152 \pm 0.045$, indicating that parity is violated in the neutral current process $e^+e^- \rightarrow \tau^+\tau^-$. The result corresponds to a ratio of the neutral current vector and axial vector coupling constants of the τ lepton $g_{V\tau}(M_Z^2)/g_{A\tau}(M_Z^2) = 0.076 \pm 0.023$ and a value of the electroweak mixing parameter $\sin^2\theta_W(M_Z^2) = 0.2302 \pm 0.0058$.

(Submitted to Physics Letters B)

The ALEPH Collaboration

D. Decamp, B. Deschizeaux, C. Goy, J.-P. Lees, M.-N. Minard

Laboratoire de Physique des Particules (LAPP), IN²P³-CNRS, 74019 Annecy-le-Vieux Cedex, France

R. Alemany, J.M. Crespo, M. Delfino, E. Fernandez, V. Gaitan, Ll. Garrido, Ll.M. Mir, A. Pacheco

Laboratorio de Fisica de Altas Energias, Universidad Autonoma de Barcelona, 08193 Bellaterra (Barcelona), Spain[8]

M.G. Catanesi, D. Creanza, M. de Palma, A. Farilla, G. Iaselli[1] G. Maggi, M. Maggi, S. Natali, S. Nuzzo, M. Quattromini, A. Ranieri, G. Raso, F. Romano, F. Ruggieri, G. Selvaggi, L. Silvestris, P. Tempesta, G. Zito

INFN Sezione di Bari e Dipartimento di Fisica dell' Università, 70126 Bari, Italy

Y. Gao, H. Hu[21] D. Huang, X. Huang, J. Lin, J. Lou, C. Qiao[21] T. Ruan[21] T. Wang, Y. Xie, D. Xu, R. Xu, J. Zhang, W. Zhao

Institute of High-Energy Physics, Academia Sinica, Beijing, The People's Republic of China[9]

W.B. Atwood[2] L.A.T. Bauerdick, F. Bird, E. Blucher, G. Bonvicini, F. Bossi, J. Boudreau, D. Brown, T.H. Burnett[3] H. Drevermann, R.W. Forty, C. Grab, R. Hagelberg, S. Haywood, J. Hilgart, B. Jost, M. Kasemann, J. Knobloch, A. Lacourt, E. Lançon, I. Lehraus, T. Lohse, A. Marchioro, M. Martinez, P. Mato, S. Menary, A. Minten, A. Miotto, R. Miquel, H.-G. Moser, J. Nash, P. Palazzi, F. Ranjard, G. Redlinger, A. Roth, J. Rothberg[3] H. Rotscheidt, M. Saich, R. St.Denis, D. Schlatter, M. Takashima, M. Talby[4] W. Tejessy, H. Wachsmuth, S. Wasserbaech, S. Wheeler, W. Wiedenmann, W. Witzeling, J. Wotschack

European Laboratory for Particle Physics (CERN), 1211 Geneva 23, Switzerland

Z. Ajaltouni, M. Bardadin-Otwinowska, R. El Fellous, A. Falvard, P. Gay, J. Harvey, P. Henrard, J. Jousset, B. Michel, J-C. Montret, D. Pallin, P. Perret, J. Proriol, F. Prulhière, G. Stimpfl

Laboratoire de Physique Corpusculaire, Université Blaise Pascal, IN²P³-CNRS, Clermont-Ferrand, 63177 Aubière, France

J.D. Hansen, J.R. Hansen, P.H. Hansen, R. Møllerud, B.S. Nilsson

Niels Bohr Institute, 2100 Copenhagen, Denmark[10]

I. Efthymiopoulos, E. Simopoulou, A. Vayaki

Nuclear Research Center Demokritos (NRCD), Athens, Greece

J. Badier, A. Blondel, G. Bonneaud, J. Bourotte, F. Braems, J.C. Brient, G. Fouque, A. Gamess, R. Guirlet, S. Orteu, A. Rosowsky, A. Rougé, M. Rumpf, R. Tanaka, H. Videau

Laboratoire de Physique Nucléaire et des Hautes Energies, Ecole Polytechnique, IN²P³-CNRS, 91128 Palaiseau Cedex, France

D.J. Candlin, E. Veitch

Department of Physics, University of Edinburgh, Edinburgh EH9 3JZ, United Kingdom[11]

G. Parrini

Dipartimento di Fisica, Università di Firenze, INFN Sezione di Firenze, 50125 Firenze, Italy

M. Corden, C. Georgiopoulos, M. Ikeda, J. Lannutti, D. Levinthal[16] M. Mermikides, L. Sawyer

Supercomputer Computations Research Institute and Dept. of Physics, Florida State University, Tallahassee, FL 32306, USA [13,14,15]

A. Antonelli, R. Baldini, G. Bencivenni, G. Bologna[5], P. Campana, G. Capon, F. Cerutti, V. Chiarella, B. D'Ettorre-Piazzoli[6], G. Felici, P. Laurelli, G. Mannocchi[6], F. Murtas, G.P. Murtas, G. Nicoletti, L. Passalacqua, M. Pepe-Altarelli, P. Picchi[5], P. Zografou

Laboratori Nazionali dell'INFN (LNF-INFN), 00044 Frascati, Italy

B. Altoon, O. Boyle, A.W. Halley, I. ten Have, J.L. Hearns, J.G. Lynch, W.T. Morton, C. Raine, J.M. Scarr, K. Smith, A.S. Thompson, R.M. Turnbull

Department of Physics and Astronomy, University of Glasgow, Glasgow G12 8QQ, United Kingdom[11]

B. Brandl, O. Braun, R. Geiges, C. Geweniger, P. Hanke, V. Hepp, W. Hermann, E.E. Kluge, J. Liebmann, Y. Maumary, A. Putzer, B. Rensch, A. Stahl, K. Tittel, M. Wunsch

Institut für Hochenergiephysik, Universität Heidelberg, 6900 Heidelberg, Fed. Rep. of Germany[17]

A.T. Belk, R. Beuselinck, D.M. Binnie, W. Cameron, M. Cattaneo, P.J. Dornan[1], S. Dugeay, A.M. Greene, J.F. Hassard, N.M. Lieske, S.J. Patton, D.G. Payne, M.J. Phillips, J.K. Sedgbeer, G. Taylor, I.R. Tomalin, A.G. Wright

Department of Physics, Imperial College, London SW7 2BZ, United Kingdom[11]

P. Girtler, D. Kuhn, G. Rudolph

Institut für Experimentalphysik, Universität Innsbruck, 6020 Innsbruck, Austria[19]

C.K. Bowdery[1], T.J. Brodbeck, A.J. Finch, F. Foster, G. Hughes, N.R. Keemer, M. Nuttall, A. Patel, B.S. Rowlingson, T. Sloan, S.W. Snow, E.P. Whelan

Department of Physics, University of Lancaster, Lancaster LA1 4YB, United Kingdom[11]

T. Barczewski, K. Kleinknecht, J. Raab, B. Renk, S. Roehn, H.-G. Sander, M. Schmelling, H. Schmidt, F. Steeg, S.M. Walther, B. Wolf

Institut für Physik, Universität Mainz, 6500 Mainz, Fed. Rep. of Germany[17]

J-P. Albanese, J-J. Aubert, C. Benchouk, V. Bernard, A. Bonissent, D. Courvoisier, F. Etienne, S. Papalexiou, P. Payre, B. Pietrzyk, Z. Qian

Centre de Physique des Particules, Faculté des Sciences de Luminy, IN^{2}P^3-CNRS, 13288 Marseille, France

H. Becker, W. Blum, P. Cattaneo, G. Cowan, B. Dehning, H. Dietl, F. Dydak[26], M. Fernandez-Bosman, T. Hansl-Kozanecka[22], A. Jahn, W. Kozanecki,[2,23] E. Lange, J. Lauber, G. Lütjens, G. Lutz, W. Männer, Y. Pan, R. Richter, J. Schröder, A.S. Schwarz, R. Settles, U. Stierlin, J. Thomas, G. Wolf

Max-Planck-Institut für Physik und Astrophysik, Werner-Heisenberg-Institut für Physik, 8000 München, Fed. Rep. of Germany[17]

V. Bertin, J. Boucrot, O. Callot[1], X. Chen, A. Cordier, M. Davier, G. Ganis, J.-F. Grivaz, Ph. Heusse, P. Janot, D.W. Kim[20], F. Le Diberder, J. Lefrançois[1], A.-M. Lutz, J.-J. Veillet, I. Videau, Z. Zhang, F. Zomer

Laboratoire de l'Accélérateur Linéaire, Université de Paris-Sud, IN^{2}P^3-CNRS, 91405 Orsay Cedex, France

D. Abbaneo, S.R. Amendolia, G. Bagliesi, G. Batignani, L. Bosisio, U. Bottigli, C. Bradaschia, M. Carpinelli, M.A. Ciocci, R. Dell'Orso, I. Ferrante, F. Fidecaro, L. Foà, E. Focardi, F. Forti, A. Giassi, M.A. Giorgi, F. Ligabue, A. Lusiani, E.B. Mannelli, P.S. Marrocchesi, A. Messineo, L. Moneta, F. Palla, G. Sanguinetti, J. Steinberger, R. Tenchini, G. Tonelli, G. Triggiani, C. Vannini, A. Venturi, P.G. Verdini, J. Walsh

Dipartimento di Fisica dell'Università, INFN Sezione di Pisa, e Scuola Normale Superiore, 56010 Pisa, Italy

J.M. Carter, M.G. Green[1], P.V. March, T. Medcalf, I.S. Quazi, J.A. Strong, R.M. Thomas, L.R. West, T. Wildish

Department of Physics, Royal Holloway & Bedford New College, University of London, Surrey TW20 OEX, United Kingdom[11]

D.R. Botterill, R.W. Clifft, T.R. Edgecock, M. Edwards, S.M. Fisher, T.J. Jones, P.R. Norton, D.P. Salmon, J.C. Thompson

Particle Physics Dept., Rutherford Appleton Laboratory, Chilton, Didcot, OXON OX11 OQX, United Kingdom[11]

B. Bloch-Devaux, P. Colas, C. Klopfenstein, E. Locci, S. Loucatos, E. Monnier, P. Perez, J.A. Perlas, F. Perrier, J. Rander, J.-F. Renardy, A. Roussarie, J.-P. Schuller, J. Schwindling, B. Vallage

Département de Physique des Particules Elémentaires, CEN-Saclay, 91191 Gif-sur-Yvette Cedex, France[18]

J.G. Ashman, C.N. Booth, C. Buttar, R. Carney, S. Cartwright, F. Combley, M. Dinsdale, M. Dogru, F. Hatfield, J. Martin, D. Parker, P. Reeves, L.F. Thompson

Department of Physics, University of Sheffield, Sheffield S3 7RH, United Kingdom[11]

E. Barberio, S. Brandt, H. Burkhardt,[1] C. Grupen, H. Meinhard, L. Mirabito, U. Schäfer, H. Seywerd

Fachbereich Physik, Universität Siegen, 5900 Siegen, Fed. Rep. of Germany[17]

G. Apollinari, G. Giannini, B. Gobbo, F. Liello, F. Ragusa,[25] L. Rolandi, U. Stiegler

Dipartimento di Fisica, Università di Trieste e INFN Sezione di Trieste, 34127 Trieste, Italy

L. Bellantoni, X. Chen, D. Cinabro, J.S. Conway, D.F. Cowen,[24] Z. Feng, D.P.S. Ferguson, Y.S. Gao, J. Grahl, J.L. Harton, J.E. Jacobsen, R.C. Jared,[7] R.P. Johnson, B.W. LeClaire, Y.B. Pan, J.R. Pater, Y. Saadi, V. Sharma, Z.H. Shi, Y.H. Tang, A.M. Walsh, J.A. Wear,[27] F.V. Weber, M.H. Whitney, Sau Lan Wu, G. Zobernig

Department of Physics, University of Wisconsin, Madison, WI 53706, USA[12]

[1] Now at CERN.
[2] Permanent address: SLAC, Stanford, CA 94309, USA.
[3] Permanent address: University of Washington, Seattle, WA 98195, USA.
[4] Also Centre de Physique des Particules, Faculté des Sciences, Marseille, France
[5] Also Istituto di Fisica Generale, Università di Torino, Torino, Italy.
[6] Also Istituto di Cosmo-Geofisica del C.N.R., Torino, Italy.
[7] Permanent address: LBL, Berkeley, CA 94720, USA.
[8] Supported by CAICYT, Spain.
[9] Supported by the National Science Foundation of China.
[10] Supported by the Danish Natural Science Research Council.
[11] Supported by the UK Science and Engineering Research Council.
[12] Supported by the US Department of Energy, contract DE-AC02-76ER00881.
[13] Supported by the US Department of Energy, contract DE-FG05-87ER40319.
[14] Supported by the NSF, contract PHY-8451274.
[15] Supported by the US Department of Energy, contract DE-FC0S-85ER250000.
[16] Supported by SLOAN fellowship, contract BR 2703.
[17] Supported by the Bundesministerium für Forschung und Technologie, Fed. Rep. of Germany.
[18] Supported by the Institut de Recherche Fondamentale du C.E.A..
[19] Supported by Fonds zur Förderung der wissenschaftlichen Forschung, Austria.
[20] Supported by the Korean Science and Engineering Foundation and Ministry of Education.
[21] Supported by the World Laboratory.
[22] On leave of absence from MIT, Cambridge, MA 02139, USA.
[23] Supported by Alexander von Humboldt Fellowship, Germany.
[24] Now at California Institute of Technology, Pasadena, CA 91125, USA.
[25] Now at Dipartimento di Fisica, Università di Milano, Milano, Italy.
[26] Also at CERN, PPE Division, 1211 Geneva 23, Switzerland.
[27] Now at University of California, Santa Cruz, CA 95064, USA.

1 Introduction

Measurements of the weak neutral current coupling constants of the different fermions are important for detailed tests of the standard model of electroweak interactions. Here we present the determination of the ratio of the neutral current vector and axial vector coupling constants of the τ lepton from a measurement of the polarization of τ leptons produced in e^+e^- collisions at the Z resonance. The τ polarization has been measured in previous experiments [1,2,3], but due to the lower centre of mass energy the sensitivity to weak interaction effects was limited. The present experiment was carried out using the ALEPH detector at the LEP collider at CERN. The data, taken during 1989 and 1990 at centre of mass energies between 88.2 GeV and 94.2 GeV, correspond to an integrated luminosity of 8.5 pb^{-1}.

2 Method

The polarization of the τ lepton is a parity violating variable defined by

$$P_\tau = \frac{\sigma_R - \sigma_L}{\sigma_R + \sigma_L}$$

where σ_R and σ_L are the cross sections for the production of right-handed and left-handed τ leptons, respectively. Due to longitudinal spin correlation $P_{\tau^+} = -P_{\tau^-}$ and by convention P_τ is defined as the polarization of the τ^-. The τ polarization depends on the initial state polarization via angular momentum conservation and on the space-time structure of the τ coupling to the initial state. The effects of initial state polarization are eliminated by averaging P_τ over all τ production angles. In the following P_τ designates this average polarization.

At the Z resonance, ignoring the small contribution from one photon exchange, the average τ polarization at tree level is given in terms of the ratio of the vector and axial vector coupling constants of the τ to the Z by

$$P_\tau = -2\frac{g_{V\tau}/g_{A\tau}}{1 + (g_{V\tau}/g_{A\tau})^2}.$$

In the standard electroweak model, $g_V/g_A = 1 - 4\sin^2\theta_w$ for a lepton, θ_w being the weak mixing angle. The inclusion of one photon exchange leads to a shift in P_τ which depends on the centre of mass energy but never exceeds $\Delta P_\tau = \pm 0.03$ in the energy range covered by this experiment.

The polarization of the τ can be determined from the angular distributions of its decay products in the τ rest frame, assuming that the charged current interaction mediating the τ decay has a V–A structure. In practice it is in most cases deduced from the energies of the τ decay products in the laboratory system which are related to these distributions. In the analysis presented here the five

major decay modes are studied: $\tau \to e\nu_e\nu_\tau$, $\tau \to \mu\nu_\mu\nu_\tau$, $\tau \to \pi\nu_\tau$, $\tau \to \rho\nu_\tau$, $\tau \to a_1\nu_\tau$. For the last mode only a_1 decay into three charged pions is considered. These decay modes comprise about 80% of all τ decays. In the following the decay distributions are described using tree level expressions. The full analysis includes $O(\alpha)$ corrections. The terms proportional to P_τ have the same sign for τ^+ and τ^-.

In the leptonic decay modes the decay angles cannot be reconstructed since there are two missing neutrinos. Only the energy distributions of the electron or the muon are measured. Neglecting the mass of the daughter lepton compared to the mass of the τ and the latter compared to the mass of the Z they are given by [4]

$$W(x) = \frac{1}{3}[4x^3 - 9x^2 + 5 + P_\tau(8x^3 - 9x^2 + 1)] .$$

The variable $x = E/E_{beam}$, or equivalently $x = p/p_{beam}$, is used throughout this paper to denote energies and momenta of particles in the laboratory system measured in units of the beam energy.

For the semihadronic decay modes the distribution of the decay angle ϑ of the hadron in the τ rest frame relative to the τ line of flight is given by [5]

$$W(\cos\vartheta) = \frac{1}{2}(1 + \alpha P_\tau \cos\vartheta) ,$$

with $\alpha = 1$ for spin 0 particles (pion) and $\alpha = (m_\tau^2 - 2m^2) / (m_\tau^2 + 2m^2)$ for spin 1 particles (ρ, a_1), where m_τ and m are the masses of the τ and of the hadronic system, respectively. The angle ϑ may be expressed in terms of the fractional hadron energy x in the laboratory system:

$$\cos\vartheta = \frac{2x - 1 - m^2/m_\tau^2}{1 - m^2/m_\tau^2} .$$

The reduction of the analysing power for hadrons of spin 1 by the factor α is due to the contribution of both longitudinal and transverse spin states of the hadron to the τ decay distribution. The spin states can be separated by introducing a second angle ψ which characterizes the decay distribution of the hadron into final state pions [6,7]. For the ρ this is the decay angle of the 2π system relative to the ρ line of flight and it is given in terms of the energies of the two pions:

$$\cos\psi = \frac{m}{\sqrt{m^2 - 4m_\pi^2}} \frac{E_\pi - E_{\pi^0}}{|\vec{p}_\pi + \vec{p}_{\pi^0}|} .$$

For the a_1, ψ is the angle between the normal to the decay plane of the 3π system in the a_1 rest frame and the a_1 line of flight [7].

The τ polarization is determined from the energy spectra in the case of the decay modes $\tau \to e\nu_e\nu_\tau$, $\tau \to \mu\nu_\mu\nu_\tau$, $\tau \to \pi\nu_\tau$ and from the distributions in the two angles ϑ and ψ for the modes $\tau \to \rho\nu_\tau$ and $\tau \to a_1\nu_\tau$. A linear combination of simulated event distributions for positive and negative helicities is fitted to the data with the polarization P_τ as a free parameter. The simulated τ pair events are generated using the Monte Carlo generator KORALZ [8], which includes QED radiative effects in the production and decay processes of the τ leptons. The events are then passed through the detector simulation, event reconstruction, and analysis programs in order to take detector resolution and acceptance effects into account. For the fit the distributions are corrected for misidentified decay modes, background events, and by the ratio of measured and simulated selection efficiencies if these were determined from data. Data and Monte Carlo distributions are averaged over the different centre of mass energies ignoring the slight energy dependence of the polarization in the fitting procedure.

The polarization analysis is not very sensitive to a precise modelling of the detector angular acceptance since the average τ polarization is to be measured. The result is, however, sensitive to the momentum and energy dependence of the event selection and identification efficiency, which must be known precisely.

3 Detector

The ALEPH detector, which is described in detail elsewhere [9], consists of an inner tracking chamber (ITC) surrounded by a time projection chamber (TPC) for the detection and measurement of charged particle tracks. Exterior to the TPC a highly segmented electromagnetic calorimeter (ECAL) is used to detect and measure energy and position of photon and electron showers. It consists of a sandwich of 45 layers of planar proportional chambers and lead plates assembled in 12 modules each in the barrel and the two endcaps of the detector. The energy and position of electromagnetic showers are measured using 3 x 3 cm cathode pads connected internally to form projective towers which subtend on average a solid angle of about 0.8° x 0.8°. Each tower is read out in three stacks of thickness 4, 9 and 9 radiation lengths. In addition all wire planes are read out individually. The ITC, TPC, and ECAL are enclosed by a superconducting solenoid which provides a homogeneous magnetic field of 1.5 Tesla for charged particle momentum measurements. Outside the coil the 120 cm thick iron return yoke is instrumented with 23 layers of 1 x 1 cm^2 streamer tubes to form the hadron calorimeter (HCAL). The presence of a streamer is recorded in each of the tubes individually. The analog signals induced by the streamers on pads are read out with a projective tower geometry. The HCAL towers cover solid angles of about 3.7° x 3.7° each. The detector is triggered by τ pair events with a measured efficiency >99.9% .

4 Particle Identification

The main sources of systematic error in the measurement of the τ polarization are background from misidentified τ decay modes and uncertainties in the momentum dependence of the decay mode selection. Background from other sources is in general small and of less importance. The separation of the different decay modes depends on the quality of particle identification. Procedures to identify electrons, photons, muons, and hadrons are described in the following. They are in part optimized for τ decays, where most of the time an isolated track is to be identified. Photons must be detected and identified with high efficiency close to a charged track, possibly accompanied by a hadronic shower in ECAL. Data are used to measure the identification efficiencies and to determine misidentification probabilities in most cases. The analysis does not distinguish between charged pions and kaons. This is accounted for in the simulation of the experiment. However, at the present level of sensitivity the presence of charged kaons could even be ignored.

Identification procedures using ECAL information require geometrical cuts: a track should not point near the insensitive region between two adjacent ECAL modules (crack) or to the region where barrel and endcap modules overlap. This is to ensure that a possible electron shower is contained in the sensitive volume of an ECAL module. Acceptance losses due to this requirement are close to 10%. Similar cuts in HCAL, which is used for π–μ separation, are not necessary since the effect of cracks on the identification efficiency is small in that case and can be easily measured.

4.1 Electron identification

Electrons are identified by means of three test variables R_T, R_L, and R_I, which are described in detail in Ref. 10. R_T and R_L are measures of the transverse and longitudinal shapes of showers in ECAL; R_T requires also a matching of the track momentum measured in the TPC and the energy deposition in ECAL. R_I measures the difference between the track ionization observed in the TPC and that expected for an electron. For electrons of momentum above 2 GeV/c all three variables are normally distributed with zero mean and unit variance. Their distributions have been determined using data taken in test beams and in e^+e^- collisions.

The momentum dependence of the identification efficiency is measured in the apparatus using e^+e^- scattering and e^+e^- pairs from two photon interactions or from photon conversion in hadronic events which give a full spectrum of momentum. An electron is tagged in these processes by the identification of its partner. The average efficiency excluding ECAL cracks and restricted to polar angles $|\cos\theta| < 0.7$ (barrel) is $\langle\varepsilon_e\rangle = 93.1\%$ with a small momentum dependence. It is in perfect agreement with the Monte Carlo prediction, the ratio R_e of measured and predicted efficiencies having a slope $dR_e/dx = (-2.6 \pm 2.7)\ x10^{-4}$. Misidentification of pions can occur when the pion trajectory overlaps with a photon shower in ECAL, a situation which depends on the type of events selected.

4.2 Photon identification

Due to the large Lorentz boost at LEP energies the decay products of the τ are confined to a narrow cone such that the photons from one or several neutral pions generate showers in ECAL which are in most cases very close to each other or to showers from charged hadrons. For the purpose of estimating systematic errors two different methods have been developed to identify photons in such a dense environment.

Both identification procedures begin with a search for local energy maxima among the towers of the first two stacks of ECAL. A maximum tower contains more energy than any of its immediate neighbours. Two definitions are used: in a strict definition neighbouring towers must have a common face (method A), whereas in a looser definition neighbouring towers share a face or a single corner (method B). Each local maximum represents the first tower of a separate cluster. It must have a distance from the impact of a charged particle of more than 4 cm if the cluster is to be considered as a photon candidate.

The full reconstruction of the clusters and the assignment of energies starts from the local maxima. In method A the remaining towers are assigned in order of decreasing energy, adding the energy of a tower to the same cluster as its highest energy neighbour. Method B shares the energy of a cell between adjacent clusters with an algorithm based on the expected radial distributions for electromagnetic showers normalized to the energies of the local maxima. Photon candidates must have clusters extending in depth over at least two stacks in order to reject satellite clusters of hadronic showers. The minimum cluster energy is 250 to 300 MeV, but in method B this threshold is raised to 1 GeV if the photon shower overlaps with a cluster that is linked to the track of a charged particle.

The efficiencies of these identification procedures and the misidentification probabilities depend on the kind of events selected. They are determined by Monte Carlo simulation. The comparison between data and Monte Carlo is shown in Fig.1(a) for the total number of reconstructed photons per τ candidate and in Fig. 1(b) for the $\gamma\gamma$ invariant mass distribution in τ candidates with two photon clusters. The latter shows a clear peak at the π^0 mass. Both distributions are very similar for the two methods. The agreement between data and simulation is satisfactory. The π^0 mass reconstruction has been used as a check of the measurement of the π^0 energy.

4.3 Separation of hadrons and muons

The pattern of streamer tube hits in HCAL is employed to distinguish hadrons from muons, making use of the characteristic penetration of muons through HCAL without interaction. Two test variables are constructed. The first is used to detect penetrating tracks by searching for tube hits in the outermost layers of HCAL. The hits must be within a few centimetres wide road, obtained by

extrapolating a track from the TPC into HCAL. The second variable is sensitive to showers in HCAL and is based on the width of the tube pattern in all planes containing hits. The width is defined as the distance between the most separated tubes hit in a plane within a 60 cm wide road. In a given decay mode the cuts on the two variables are chosen such that the acceptance is optimized while keeping the background contribution to the systematic error on the polarization small compared to the other errors. For this purpose test samples of muons and hadrons are selected from data, which are identified without using HCAL information. They are used to measure the energy dependence of the identification efficiency and to determine the misidentification probability.

To select muons for a test sample, charged tracks are required to have associated hits in the muon chambers. Alternatively muons from $\mu^+\mu^-$ pair events are identified by the second muon and kinematic cuts. Identified charged pions are mainly obtained from the decay $\tau^\pm \to \rho^\pm \nu_\tau$ with $\rho^\pm \to \pi^\pm\pi^o$, where the charged track is identified by the accompanying π^o, which in turn is identified by its invariant mass calculated from photon candidates in ECAL.

The muon identification efficiency ε_μ, averaged over polar angles with respect to the beam axis in the range $|\cos\theta| < 0.9$, is almost independent of energy for $x>0.1$. The average over energies is $\langle\varepsilon_\mu\rangle = 0.847 \pm 0.003$ with a slope of $d\varepsilon_\mu/dx = 0.024 \pm 0.012$. The efficiency includes losses due to HCAL cracks. The probability of misidentifying hadrons, averaged over the spectrum of the test sample, amounts to $(1.0\pm 0.3)\%$. No significant energy dependence is observed. The spectra of both the test sample and the semihadronic one prong τ decays are rather similar in shape.

The identification efficiency of hadrons using the two variables for penetration and shower width exhibits a strong momentum dependence and rises typically by a factor of 2 between 3 GeV and 30 GeV. This behaviour is mainly due to the cut on the shower width, which removes in particular low energy hadrons. These can in part be recovered by accepting events which, after passing the criterion for a non-penetrating track, failed the shower width cut, but have a charged track interacting in ECAL. The condition for a hadronic interaction is that the track is minimum ionizing in the front part of ECAL and that the energy deposition of the track in the rear part of ECAL exceeds the average signal from a muon by a factor of 3. This latter part of the identification procedure cannot be checked with the hadron test sample described above, since ECAL was used to select the events. Data from the exposure of an ECAL module to a test beam of pions [11], taken at energies of 5, 7, 10, 20, and 30 GeV, are used instead. The identification efficiency for hadrons obtained by combining the three criteria varies between 80% and 95% for fractional momenta $x > 0.1$, the range used in the final analysis for the decay mode $\tau \to \pi\nu_\tau$. The efficiency predicted from simulated events differs by about 4%. However, only the momentum dependence is important here and this is in good agreement with the data. If the ratio R_h of measured and predicted efficiencies is fitted linearly with x one finds $dR_h/dx = 0.018 \pm 0.052$. The probability of misidentifying muons has been determined to be $(0.32 \pm 0.08)\%$ from the muon test sample.

5 Event selection and analysis

In a first step Z candidates decaying into lepton pairs are selected. An event should have between two and six tracks with momenta greater than 0.1 GeV/c coming from the interaction point, and at least one track with momentum greater than 3 GeV/c. The event is divided into two jets of tracks by a plane perpendicular to the thrust axis and it is required that there should be at least one track in each jet. The jets should be narrow such that there is no track in the event with an angle greater than 18.2 degrees with respect to the axis of its jet. The acollinearity angle between the two jet axes is required to be less than 26 degrees. After these cuts the sample contains mainly lepton pairs with a small background from cosmic ray muons, two photon interactions, and hadronic Z decays.

In a second step individual τ decay modes are selected from the lepton sample. Jet topologies with either one prong or three prongs are considered. Polar angles of the jet are restricted to the range $|\cos\theta| < 0.9$, where track momenta and showers in the calorimeters are well measured. An exception is made for the decay $\tau \rightarrow e\, \nu_e \nu_\tau$, where $|\cos\theta| < 0.7$ because of the large background from Bhabha events at small scattering angles. Backgrounds from other than τ pair final states are further reduced in the step of decay mode selection. In particular, background from hadronic Z decays and cosmic rays is reduced to a negligible level.

5.1 $\tau \rightarrow e\, \nu_e \nu_\tau$

Candidates for the decay $\tau \rightarrow e\, \nu_e \nu_\tau$ are one prong jets identified as electrons. The electron energy has to be greater than 2 GeV. A sizeable fraction of the energy of electrons can be radiated in the material of the detector. Therefore the sum of the electron and photon energies as measured in ECAL is used as an estimate of the electron energy. To ensure a good energy measurement and electron identification the momentum vector of a track at both the interaction point (for radiated photons) and the entrance to ECAL (for the electron) should not point in the vicinity of an ECAL crack. This requirement holds also for the recoil jet in order to allow for an efficient identification and rejection of Bhabha events.We require that there be only one identified electron in the event and that the ECAL energy x_r of the recoil jet be less than 0.75. The remaining Bhabha background amounts to $(0.85 \pm 0.50)\%$ concentrated at $x > 0.9$. The background from two photon interactions is reduced to a negligible level by requiring the maximum acollinearity angle to be less than 14.3 degrees and the transverse momentum of the recoil jet to be greater than 2 GeV/c. Misidentified hadrons are reduced by allowing for tube hits in at most two planes of HCAL within a $\pm$ 30 cm wide road with respect to the extrapolated track. The remaining background from misidentified hadrons is mainly due to $\rho^\pm \rightarrow \pi^\pm\pi^\circ$ events, where the charged track of the $\pi^\pm$ overlaps in ECAL with photons from the π°. This background is determined by simulation and found to be $(1.7 \pm 0.8)\%$ confined to $0.4 < x < 0.8$. The overall acceptance is 32%.

The resulting electron energy spectrum from 843 selected events and the background are shown in Fig.2, as well as the fit to the data. It should be pointed out that the measured energy spectrum refers to the sum of the energies of the electron and radiated photons. This has the advantage that in the polarization analysis of the spectrum one is less dependent on the detailed modelling of the radiative corrections, which are substantial in this decay mode. The fit yields

$$P_\tau = -0.36 \pm 0.17 \pm 0.06 .$$

The first error is statistical, the second error is systematic; details are given in Table 1. The dominant systematic error is due to the uncertainty in the electron identification efficiency.

5.2 $\tau \rightarrow \mu \nu_\mu \nu_\tau$

Candidates for the decay $\tau \rightarrow \mu \nu_\mu \nu_\tau$ are one prong jets identified as muons with a fractional energy $x > 0.1$. Background from μ-pair events produced in Z decays or two photon interactions is suppressed by allowing for only one identified muon in the event and by requiring the fractional momentum x_r of the recoil jet to be less than 0.75. An additional cut against events from two photon interactions requires less than 20 GeV energy in the calorimeter of the luminosity monitor close to the beam axis. The identification procedure used to search for more than one muon is based on a weaker penetration criterion with an identification efficiency of 95.5% compared to only 84.7% for the standard procedure. The events with only one out of two muons identified are estimated from the measured rate of events with two identified muons and the measured identification efficiency. A fraction of $(3.1 \pm 1.1)\%$ of the selected events are due to this type of event, about 60% of which originate from τ pairs with both particles of the pair decaying into a muon. The contamination of the sample by misidentified hadrons is determined by folding the measured probability of misidentifying hadrons as quoted in section 4.3 with a simulated spectrum of hadrons from one prong τ decays, yielding a contamination of $(3.7 \pm 1.2)\%$. The overall acceptance is 45%.

Figure 3 shows the muon spectrum of 1401 selected events together with the background from hadrons and μ pairs. The polarization was determined from a fit using simulated event distributions, but also by fitting a semi-analytical calculation [12] to the muon spectrum. The advantage of the latter approach is that there is no error contribution from the statistics of simulated events. The two fitting methods yield the same result within the statistical error of the simulated events. The final result is taken from the fit with the semi-analytical calculation.

$$P_\tau = -0.19 \pm 0.13 \pm 0.06$$

is obtained, where the dominant systematic error is the uncertainty on the fraction of misidentified hadrons.

5.3 $\tau \rightarrow \pi \nu_\tau$

The main task in the selection procedure for the decay $\tau \rightarrow \pi\nu_\tau$ is to remove events where an isolated charged hadron is accompanied by one or several neutral pions. The presence of a shower which develops in the first few radiation lengths of ECAL is a signature for this type of event.Two methods are employed to detect an early shower development in the vicinity of a track. They use the signals from the wire planes of the ECAL module hit by the track and all its neighbour modules. The methods also detect and remove electrons, whereas π–μ separation to fully identify hadrons is applied in a later step.

Method A detects the beginning of a shower from the energy profile of the wire planes. An energy deposition exeeding the average signal from a minimum ionizing particle by a factor of 2.5 in three consecutive wire planes indicates the start of a shower. There should be no shower starting before five radiation lengths. In method B the energy sum in the first four radiation lengths is required to be less than 350 MeV, which corresponds to about four times the signal of a minimum ionizing particle. This main cut in method B is supplemented by either of two requirements which reduce the signal by only 4% but the remaining background by more than a factor of 2: (i) The energy deposit in the first two stacks of ECAL as determined from the towers along the track trajectory and the sum of the wire signals in the corresponding module and its neighbours should be compatible with that of a minimum ionizing particle; or (ii) there should be no isolated ECAL cluster with energy above 500 MeV in the hemisphere around the track.

Tracks passing these cuts are due to pions, kaons, and muons, with a small contamination of electrons and hadrons accompanied by undetected photons. Some misidentified ρ and K^* final states are rejected by demanding the total calorimetric energy - from ECAL and HCAL - around the extrapolated track direction to be less than twice the momentum of the track.

The selection efficiencies due to the cut of method A and due to the main cut in method B are determined from the pion test beam data [11] at energies between 5 GeV and 30 GeV. They are extrapolated to the highest energies of about 47 GeV. The selection efficiencies are about 70% for method A and 75% for method B. To estimate the uncertainty in the energy dependence, the ratio R_E of the measured and simulated efficiencies is fitted to a straight line in the fractional energy x. The error on the slope dR_E/dx is $\pm$ 0.030, which translates into an error in the polarization of $\pm$ 0.015.

The muons in the remaining sample are removed by the π–μ separation procedure described in section 4.3. To reduce events from two photon interactions the more energetic of the two jets has to have a fractional momentum $x > 0.1$. To further reduce background from μ pair events, an event is rejected if the recoil jet is an identified muon with $x_r > 0.75$. Bhabha events are further suppressed by

rejecting events where the energy deposition in ECAL in one hemisphere of the event is greater than 80% of the beam energy.

Figure 4 shows the spectrum of pion candidates as well as the total background obtained with method A. Corrections for acceptance and background are relatively large at low x. In order to reduce systematic uncertainties due to these corrections only events with $x > 0.1$ and $x > 0.15$ for methods A and B, respectively, are used in the polarization analysis. For the two analyses 805 and 879 candidate events are retained, with 632 events common to both samples. The overall acceptance is 37% for both methods. The background due to misidentified τ decay modes has been calculated from simulated events and amounts to 5.3% and 8.5%, mainly due to the ρ and K^* final states. Backgrounds from electron pair and μ pair events are determined from data to be $(0.7 \pm 0.3)\%$. The fit results yield an average for the two samples of

$$P_\tau = -0.130 \pm 0.065 \pm 0.044 \, .$$

The difference between the two samples is $\Delta P_\tau = 0.045 \pm 0.046$. The error on ΔP_τ is predominantly statistical since the sources of systematic errors on the two methods are the same. This systematic error contains several contributions which are similar in magnitude, none of them being dominant.

5.4 $\tau \rightarrow \rho \nu_\tau$

Candidates for the decay $\tau \rightarrow \rho\nu_\tau$ are one prong jets accompanied by one or two photon clusters in a cone of 30 degrees around the track. Two samples are selected using the photon reconstruction methods described in section 4.2. Background from two photon interactions is reduced by requiring at least 2.5 GeV for the transverse momenta of the jets in the two hemispheres of the event. Bhabha and μ pair events enter the candidate samples only if they are accompanied by radiated photons. Bhabha events are reduced by demanding the total ECAL energy to be less than 80% of the centre of mass energy. The background from these sources remaining after the ρ selection cuts is negligible.

In events with two photon candidates the two photon system should have an invariant mass in the range $0.08 < m_{\gamma\gamma} < 0.20$ GeV/c^2 to be accepted as a π° candidate. The reconstructed π° is used to tag the charged particle to be a hadron; no further particle identification is employed in this case. At π° energies below 2 GeV and above 15 GeV, π° decays with only one reconstructed cluster dominate. At low energies one of the two photons is often lost due to cuts in the reconstruction algorithms, whereas at high energies the two photons merge into a single unresolved cluster. The loss of a photon results in a degradation of the reconstructed kinematics. A single cluster ia accepted as a π° candidate if its energy is greater than 4 GeV. This requirement ensures a reliable treatment of

resolution effects and backgrounds. Furthermore, in single photon cluster events the charged particle should not be identified as an electron or muon.

The π^o candidate is combined with the charged particle, assumed to be a pion, and the invariant mass of this system is calculated. The resulting distribution is shown in Fig.5. It is dominated by the ρ resonance above a small background entirely due to the misidentification of other τ decay modes (more than 80% from the $\pi\pi^o\pi^o$ and K^* final states). For the final analysis, the invariant mass is required to be in the range $0.5 < m_{\pi\pi} < 1.2$ GeV/c^2.

The overall acceptances for the two samples using the photon reconstruction methods A and B of section 4.2 are 46% and 50%, yielding 2001 and 2184 events, respectively, with about 1700 events in common. The fraction of background events as determined by Monte Carlo amounts to 8.1% and 10.5%. The event distributions in $\cos\psi$ for different bins in $\cos\vartheta$ are displayed in Fig.6 for method B together with the background and the fit result. The average of the two results is

$$P_\tau = -0.124 \pm 0.047 \pm 0.051$$

and the difference $\Delta P_\tau = 0.082 \pm 0.034 \pm 0.041$. This difference indicates that the systematic errors from the photon reconstruction are larger than our estimates. The systematic error on P_τ has been increased to take this into account.

5.5 $\tau \rightarrow a_1 \nu_\tau$

The analysis starts from events with a three prong jet. Jets with at least one track identified as an electron are rejected to eliminate events with converted photons. Then ECAL is searched for photons coming from neutral pions in a cone of 30 degrees around the jet axis. We observe 1128 3π candidates (sample A) and 748 $3\pi+\geq 1\gamma$ candidates (sample B) which were used to study the background in sample A. The residual electron pair contamination in the three prong sample is less than 1%.

The Dalitz plots and the 3π mass spectra for the two samples display very different characteristics (Fig.7). Sample A is compatible with pure $a_1 \rightarrow \rho^o\pi$. In sample B the 3π mass spectrum is broader and the population of the Dalitz plot is concentrated in the low mass region. A cut on the mass of the 3π system $m_{3\pi} < 1.6$ GeV/c^2 removes badly measured events and possible background from hadronic Z decays. To reduce background of the type of sample B, but with undetected photons, a further cut requires that at least one of the two $\pi^+\pi^-$ masses satisfies the condition for a ρ: $0.36 < m^2 < 0.81$ (GeV/c^2)^2. The remaining background is estimated by Monte Carlo to be (6.5 ± 1.6)%. The error is systematic and has been obtained by comparing the Dalitz plot

for data and Monte Carlo in the corner $m^2 < 0.32$ $(GeV/c^2)^2$. After all cuts sample A contains 990 events, the overall acceptance being 55%.

When fitting the two-dimensional distributions one faces the problem of statistical fluctuations of the simulated events in sparsely populated regions of the phase space, making large samples of simulated events necessary. This can be avoided by jointly fitting three moments of the two variables instead, without losing significantly in analyzing power [13]: $\langle\cos\vartheta\rangle$, $\langle 3\cos^2\psi - 1\rangle$, and $\langle\cos\vartheta(3\cos^2\psi - 1)\rangle$. This has been done for the a_1 decay mode. The result is

$$P_\tau = -0.15 \pm 0.15 \pm 0.07 \, .$$

Figure 8 shows the distributions of the events and of the moment $\langle 3\cos^2\psi - 1\rangle$ as functions of $\cos\vartheta$. The sensitivity to the polarization of the τ is derived almost entirely from the second distribution. An important point to note is that the acceptance is constant in $\cos\psi$ within errors, making the result rather independent of the simulation of this decay mode.

6 Results

The results of the polarization analyses are summarized in Table 1. The fitted event distributions are compared to the data in Figs. 2, 3, 4, 6, and 8. The weighted average of the polarization obtained from all five decay modes is $P_\tau = -0.150 \pm 0.045$. The statistical and systematic errors have been added in quadrature. Correlations between τ decays in the same event and between the systematic errors of the different decay modes are negligible. For further analysis it is convenient to quote P_τ at an effective centre of mass energy equal to M_Z. The corrections for the energy dependence of P_τ and for initial state radiation is small. The final value is

$$P_\tau = -0.152 \pm 0.045 \, .$$

The measured value for the τ polarization differs from zero by more than three standard deviations. This is the first observation of a non-zero lepton polarization produced in e^+e^- annihilation. This result implies that (i) parity is violated in the process $e^+e^- \to \tau^+\tau^-$ and (ii) parity is violated in the considered τ decays, without which a τ polarization could not be observed. Parity violation in the weak neutral current has been previously reported in polarized electron inelastic scattering [14] and in atomic transitions [15]. The present result extends this observation to the τ lepton, in agreement with the universality of the electroweak theory. As for parity violation in τ decays, our finding confirms the recent observation in the decay $\tau \to 3\pi\nu_\tau$ [16].

In the framework of the improved Born approximation [17] the τ polarization may be interpreted in terms of the running coupling constants $g_{V\tau}(\mu^2)$ and $g_{A\tau}(\mu^2)$ at $\mu = M_Z$, replacing $g_{V\tau}$ and $g_{A\tau}$ in the tree level formula

$$P_\tau = -2\,\frac{g_{V\tau}/g_{A\tau}}{1+(g_{V\tau}/g_{A\tau})^2}\,.$$

Using $P_\tau = -0.152 \pm 0.045$ one obtains

$$g_{V\tau}(M_Z^2) / g_{A\tau}(M_Z^2) = 0.076 \pm 0.023\,.$$

The relation $g_{V\tau}(M_Z^2) / g_{A\tau}(M_Z^2) = 1 - 4(\sin^2\theta_w(M_Z^2) + C)$, where $C = 0.0007$ accounts for the flavour dependent weak corrections [18], yields

$$\sin^2\theta_w(M_Z^2) = 0.2302 \pm 0.0058.$$

One may combine this measurement of $g_{V\tau}/g_{A\tau}$ with the separate measurement of the partial width of the decay $Z \rightarrow \tau^+\tau^-$ from this experiment, $\Gamma_\tau = (82.3 \pm 1.6)$ MeV [19], to separate $g_{V\tau}$ and $g_{A\tau}$. With

$$\Gamma_\tau = \frac{G_F M_Z^3}{6\sqrt{2}\pi}\,(g_{V\tau}^2(M_Z^2) + g_{A\tau}^2(M_Z^2))$$

one obtains, assuming $g_{A\tau}$ is negative,

$$g_{V\tau}(M_Z^2) = -0.038 \pm 0.012,$$
$$g_{A\tau}(M_Z^2) = -0.497 \pm 0.005.$$

The absolute value of $g_{A\tau}(M_Z^2)$ is in agreement with the prediction of the standard model, which is close to 0.5. The magnitude of $g_{V\tau}$ is measured to 30% and the value of $\sin^2\theta_w(M_Z^2)$ derived from it agrees with other measurements [19], which also means that $g_{V\tau}$ behaves as expected in the standard model. This determination of the neutral current coupling constants of the τ lepton may be compared to previous results obtained at lower energies, where a combined analysis of all experiments yields $g_{V\tau} = -0.09\ ^{+0.25}_{-0.28}$ and $g_{A\tau} = -0.484 \pm 0.034$ [20]. The improvement in precision by the present experiment is about an order of magnitude.

Table 1: Summary of τ polarization analysis

Decay mode	$e\nu_e\nu_\tau$	$\mu\nu_\mu\nu_\tau$	$\pi\nu_\tau$	$\rho\nu_\tau$	$a_1\nu_\tau$
P_τ	–0.36	–0.19	–0.130	–0.124	–0.15
Statistical error	0.17	0.13	0.065	0.047	0.15
Systematic errors:					
Acceptance	0.040	0.022	0.031	0.042	negl.
Energy calibration	0.020	0.005	0.004	0.019	negl.
Misidentified τ decays	0.025	0.038	0.022	0.006	0.005
Background events	0.013	0.028	0.008	negl.	negl.
MC statistics	0.030	0.020*)	0.020	0.020	0.070
Total systematic error	0.061	0.056	0.044	0.051	0.070

*) Estimated systematic error of the semi-analytical calculation of Ref.12 used in the fit.

Acknowledgements

We wish to congratulate and thank our colleagues in the LEP division for operating the LEP storage ring with continuously improving performance. We thank also the engineers and technicians in all our institutions for their support in constructing ALEPH. Those of us from non-member countries thank CERN for its hospitality.

References

1. CELLO Collaboration, H.J. Behrend et al., Phys. Lett. B127 (1983) 270.
2. MAC Collaboration, W.T. Ford et al., Phys. Rev. D36 (1987) 1971.
3. AMY Collaboration, M.H. Lee et al., KEK Preprint 90-70 (1990).
4. G. Goggi, Proc. of the LEP Summer Study, Les Houches and CERN, 1978, CERN report 79-01 (1979) Vol.2, p.483.
5. Y.S. Tsai, Phys. Rev. D4 (1971) 2821.
6. K. Hagiwara, A.D. Martin, and D. Zeppenfeld, Phys. Lett., B235 (1990) 198.
7. A. Rougé, Z. Phys. C48 (1990) 75.
8. S. Jadach and Z. Was, Comput. Phys. Commun. 36 (1985) 191; see also Monte Carlo Group Report in "Z Physics at LEP", CERN Report 89-08 (1989) Vol. III, p.1.
9. ALEPH Collaboration, D. Decamp et al., Nucl. Instr. and Methods A286 (1990) 121.
10. ALEPH Collaboration, D. Decamp et al., Phys. Lett. B244 (1990) 551.
11. G. Bagliesi et al., Nucl. Instr. and Methods A286 (1990) 61.
12. S. Jadach and Z. Was, in "Z Physics at LEP", CERN Report 89-08 (1989) Vol. I, p.235.
13. A. Rougé, Workshop on Tau Lepton Physics, Orsay, 24-27 September 1990.
14. C. Prescott et al., Phys. Lett. B77 (1978) 347.
15. L.M. Barkov and M.S. Zolotorev, JETP Lett. 31 (1978) 357; Phys. Lett. B85 (1979) 308.
16. ARGUS Collaboration, H. Albrecht et al., Phys. Lett. B250 (1990) 164.
17. M. Consoli, W. Hollik, and F. Jegerlehner, in "Z Physics at LEP", CERN Report 89-08 (1989) Vol. I, p.7.
18. D.Bardin, W.Hollik, and T.Riemann, Z. Phys. C49 (1991) 485.
19. ALEPH Collaboration, D.Decamp et al., "Improved Measurement of Electroweak Parameters from Z decays into Fermion Pairs", submitted to Z. Phys. C.
20. S.Odaka, Workshop on Tau Lepton Physics, Orsay, 24-27 September 1990; see also KEK Preprint 90-164 (1990).

Figure captions

Fig.1: Photon reconstruction in τ events. Data are shown as dots, Monte Carlo events as histograms: (a) Total number of reconstructed photons per τ candidate (method B); the shaded histogram indicates the expected multiplicity for the $\rho^{\pm}$ final state. (b) $\gamma\gamma$ invariant mass in τ candidates with two photons (method A).

Fig.2: Total electromagnetic energy observed in candidates for the decay $\tau \rightarrow e\nu_e\nu_\tau$ in units of the beam energy: data (points with error bars), background (shaded histogram), and fitted Monte Carlo distribution (solid line) with the components due to positive (dotted line) and negative (dashed line) τ helicities.

Fig.3: Momentum of the muon in the decay $\tau \rightarrow \mu\nu_\mu\nu_\tau$ in units of the beam momentum: data (points with error bars), background (shaded histogram), and fit result (solid line, semi-analytical calculation) with the components due to positive (dotted line) and negative (dashed line) τ helicities.

Fig.4: Fractional energy of pion candidates in the decay $\tau \rightarrow \pi\nu_\tau$ (method A): data (points with error bars), background (shaded histogram), and fitted Monte Carlo distribution (solid line) with the components due to positive (dotted line) and negative (dashed line) τ helicities.

Fig.5: Invariant mass of $\pi^{\pm}\pi^{o}$ candidates selected for the decay $\tau \rightarrow \rho\nu_\tau$ (before mass cuts) from photon reconstruction method A: data (points with error bars), Monte Carlo prediction (histogram), and expected background (shaded histogram).

Fig.6: Distribution of $\cos\psi$ for different bins in $\cos\vartheta$ in the decay $\tau \rightarrow \rho\nu_\tau$ (method B): data (points with error bars), background (shaded histograms), and fitted Monte Carlo distribution (solid lines) with the components due to positive (dotted lines) and negative (dashed lines) τ helicities.

Fig.7: Characteristics of three-prong τ decays: Dalitz plot and 3π invariant mass for events without reconstructed photons (a and c) and for events with at least one reconstructed photon (b and d).

Fig.8: Distributions of (a) events in $\cos\vartheta$ and of (b) the moment $\langle 3\cos^2\psi - 1\rangle$ as a function of $\cos\vartheta$ in the decay $\tau \rightarrow 3\pi\nu_\tau$: data (points with error bars) and fitted Monte Carlo distributions (solid lines) with the components due to positive (dotted lines) and negative (dashed lines) τ helicities.

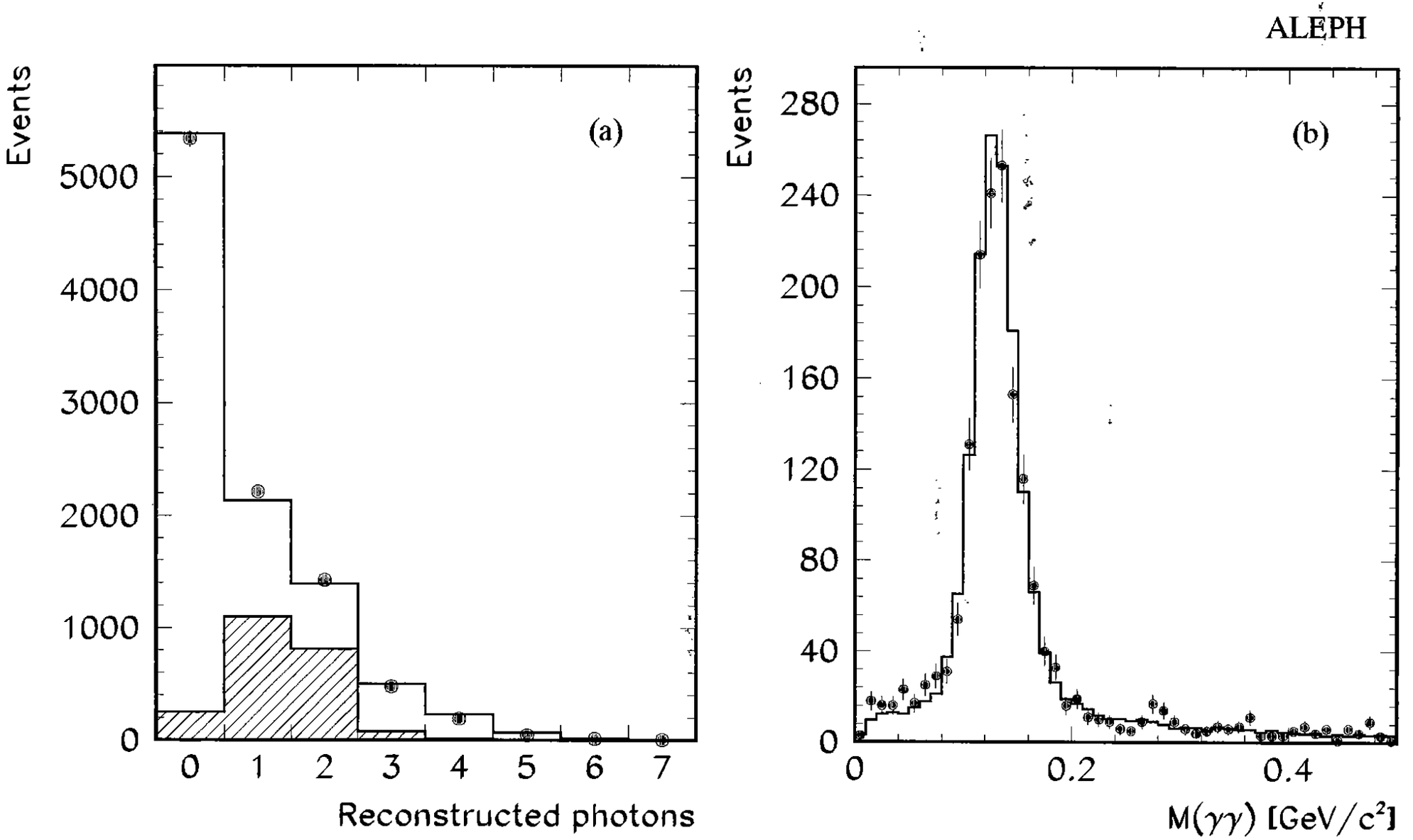
ALEPH
Events
(a)
5000
4000
3000
2000
1000
0
0 1 2 3 4 5 6 7
Reconstructed photons
Events
(b)
280
240
200
160
120
80
40
0
0 0.2 0.4
M(γγ) [GeV/c²]

Fig.1

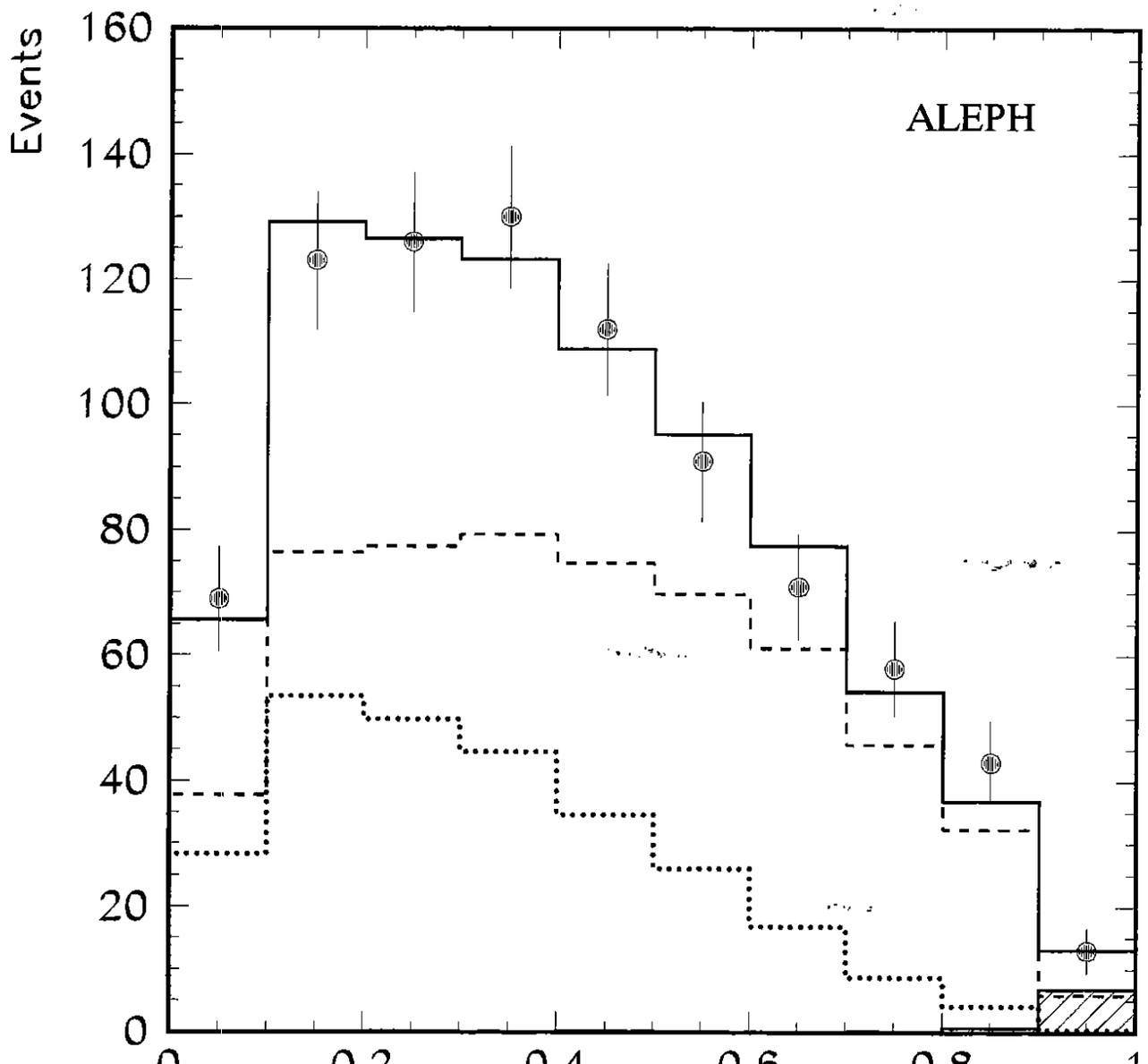

Fig.2

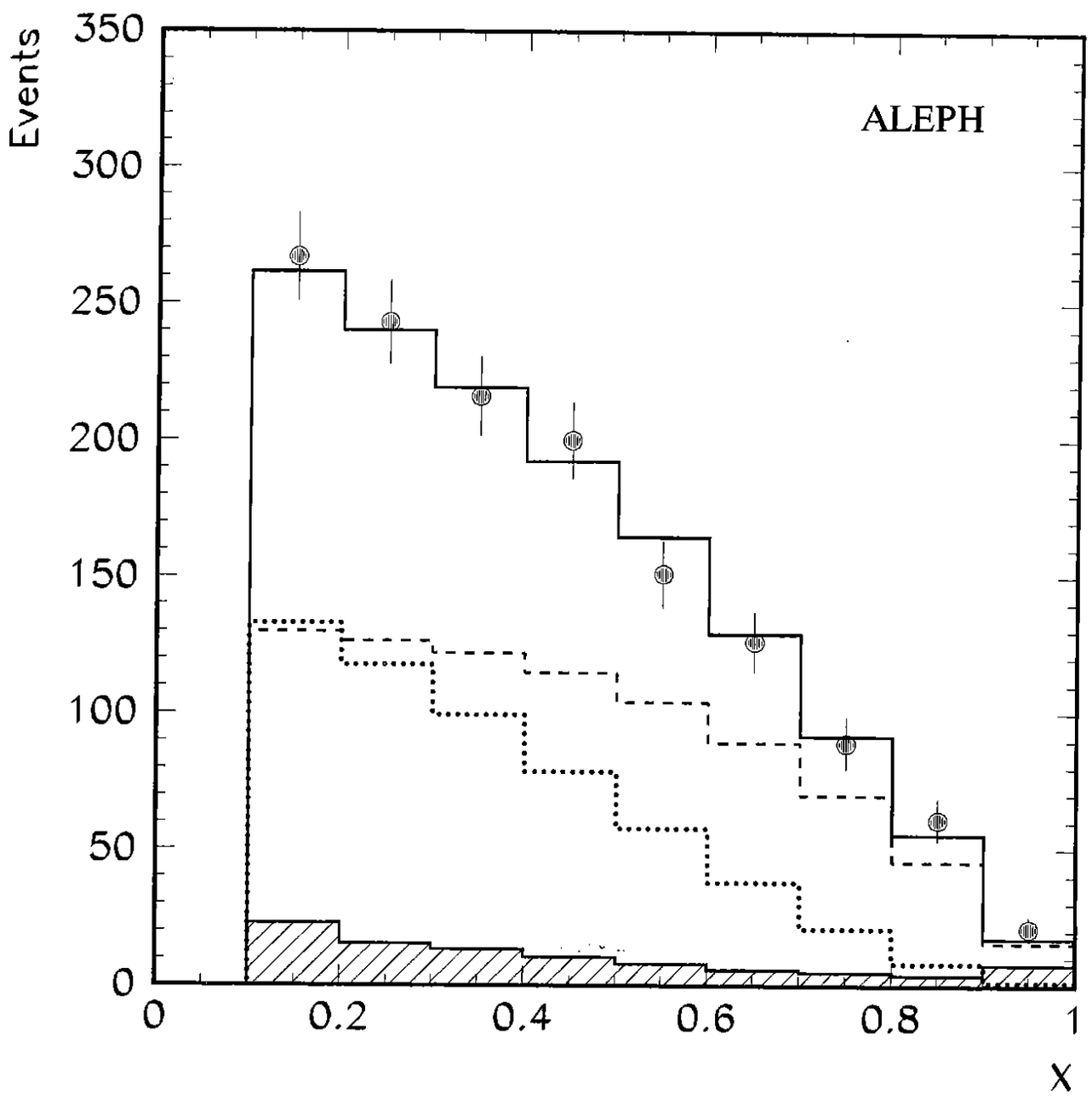

Fig.3

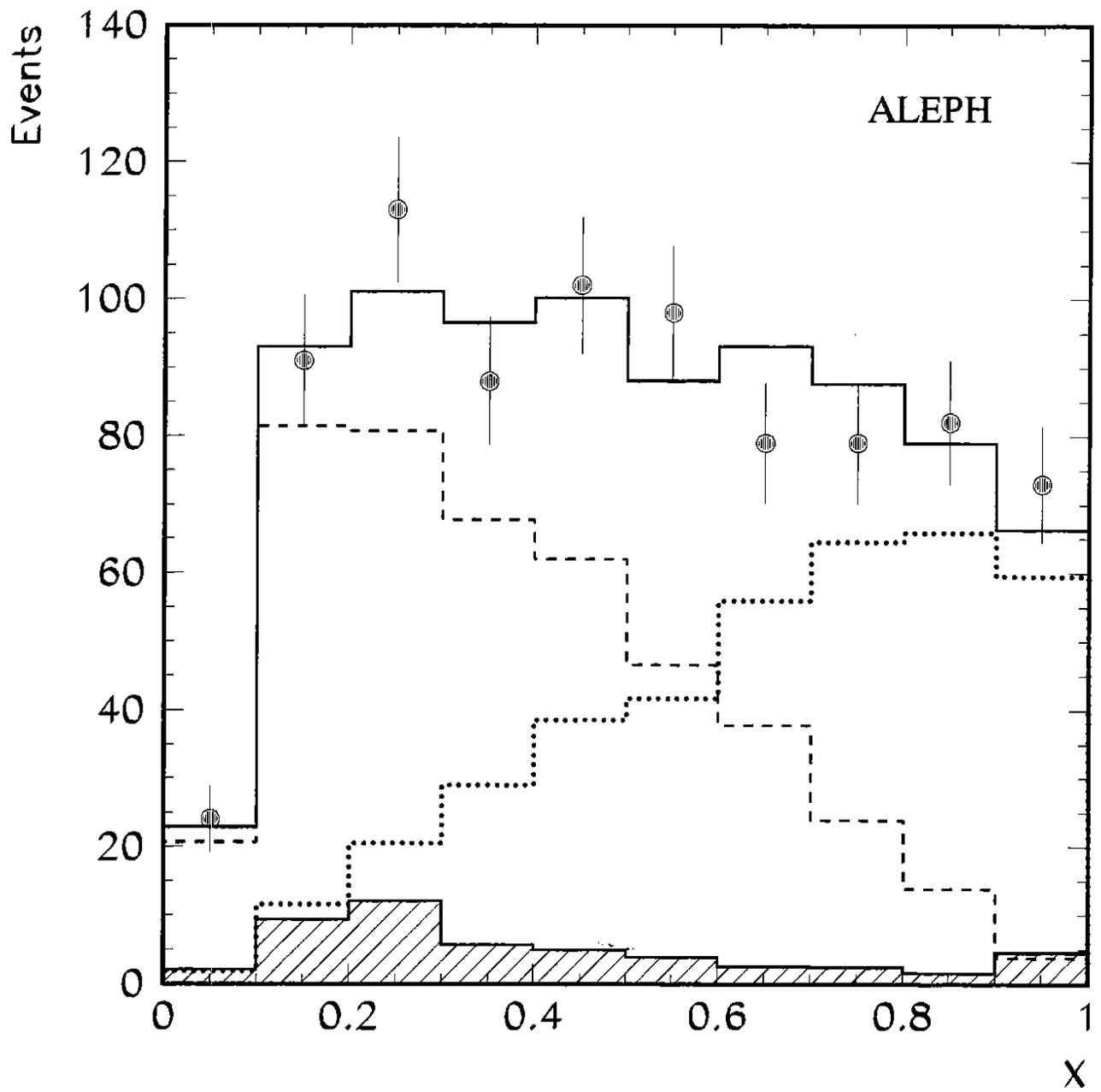

Fig.4

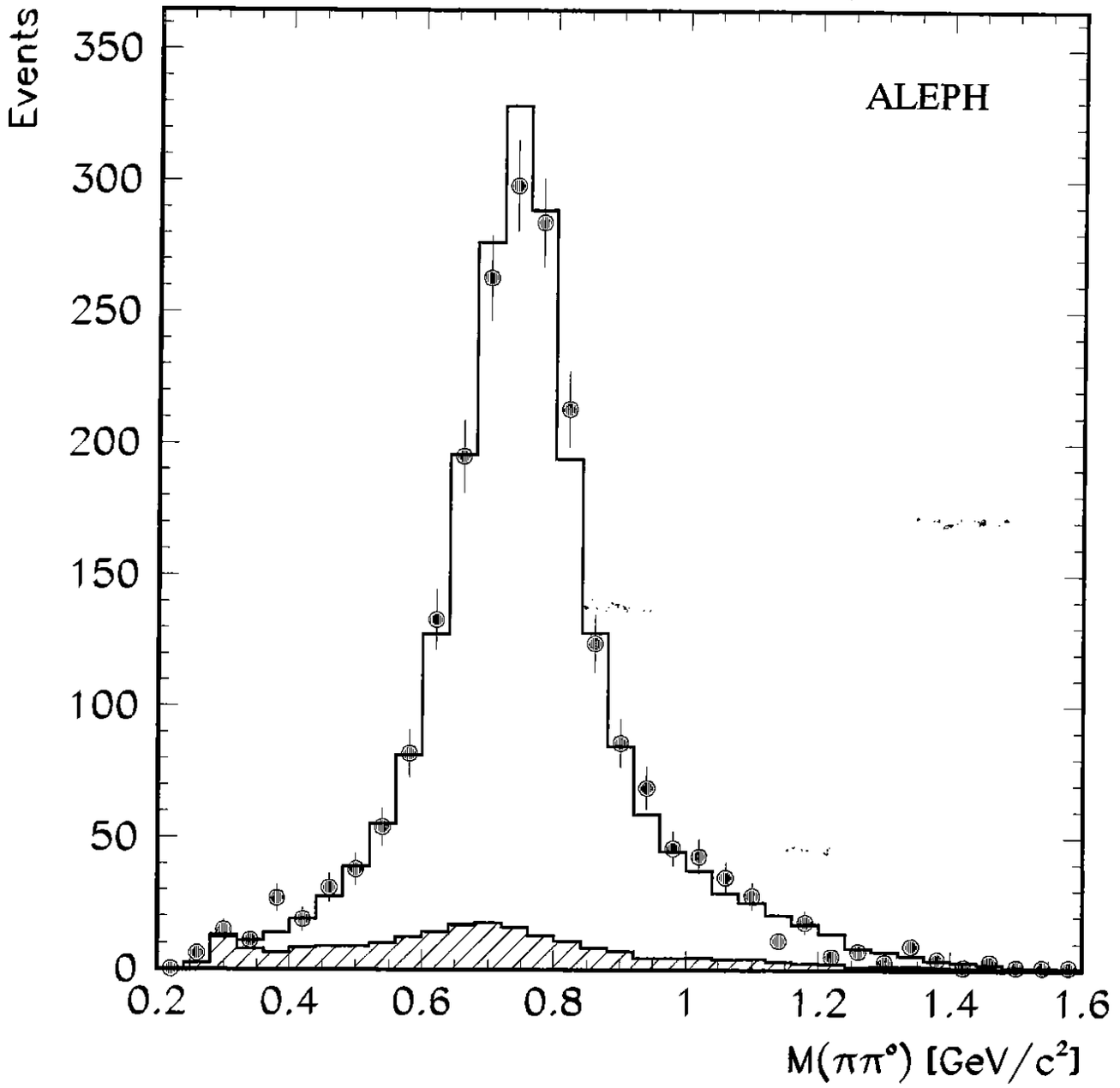
Events
350
300
250
200
150
100
50
0
ALEPH
0.2
0.4
0.6
0.8
1
1.2
1.4
1.6
M(ππ°) [GeV/c²]

Fig.5

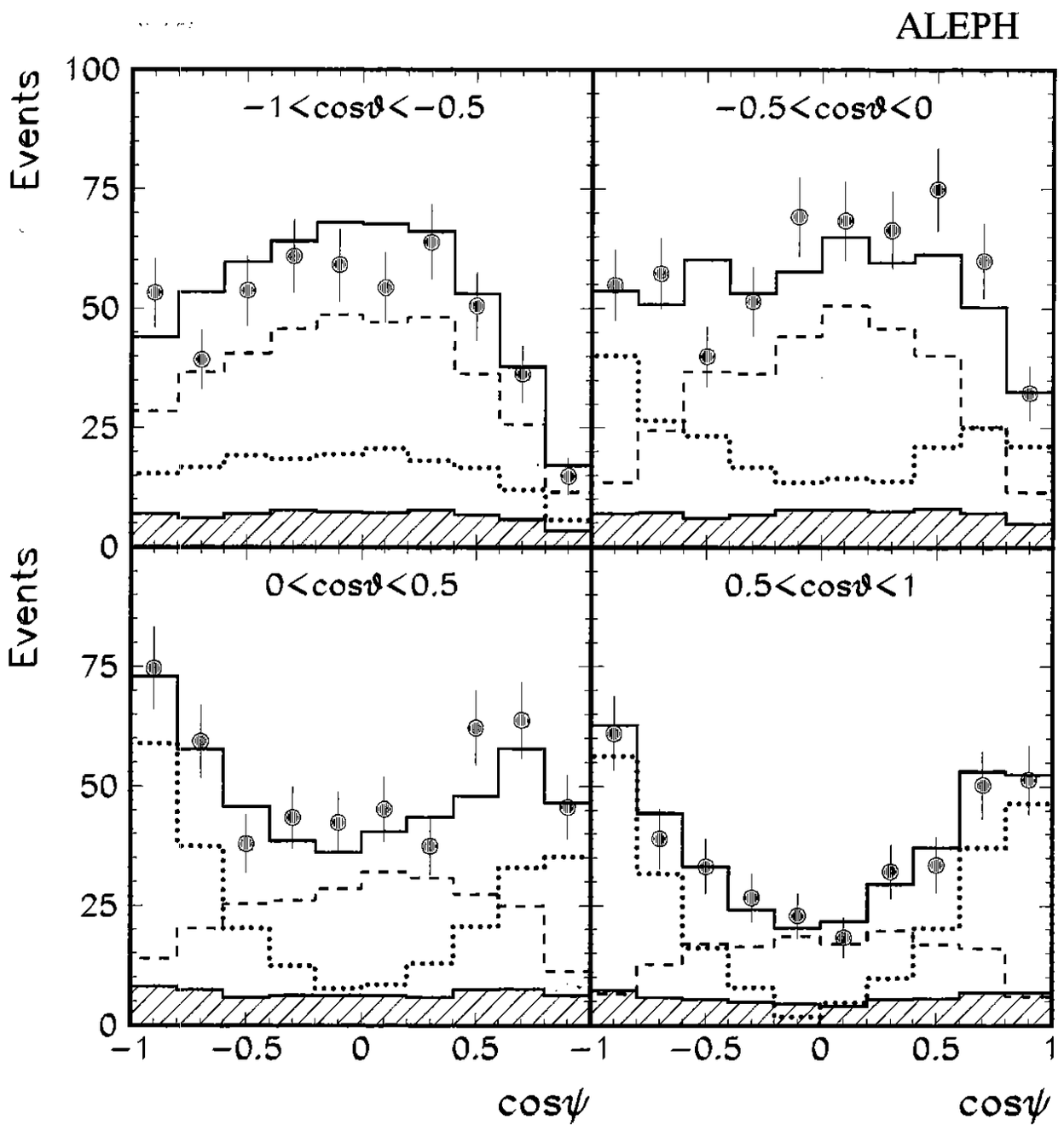
ALEPH
Events
100
75
50
25
0
−1<cosϑ<−0.5
−0.5<cosϑ<0
0<cosϑ<0.5
0.5<cosϑ<1
−1
−0.5
0
0.5
1
cosψ

Fig.6

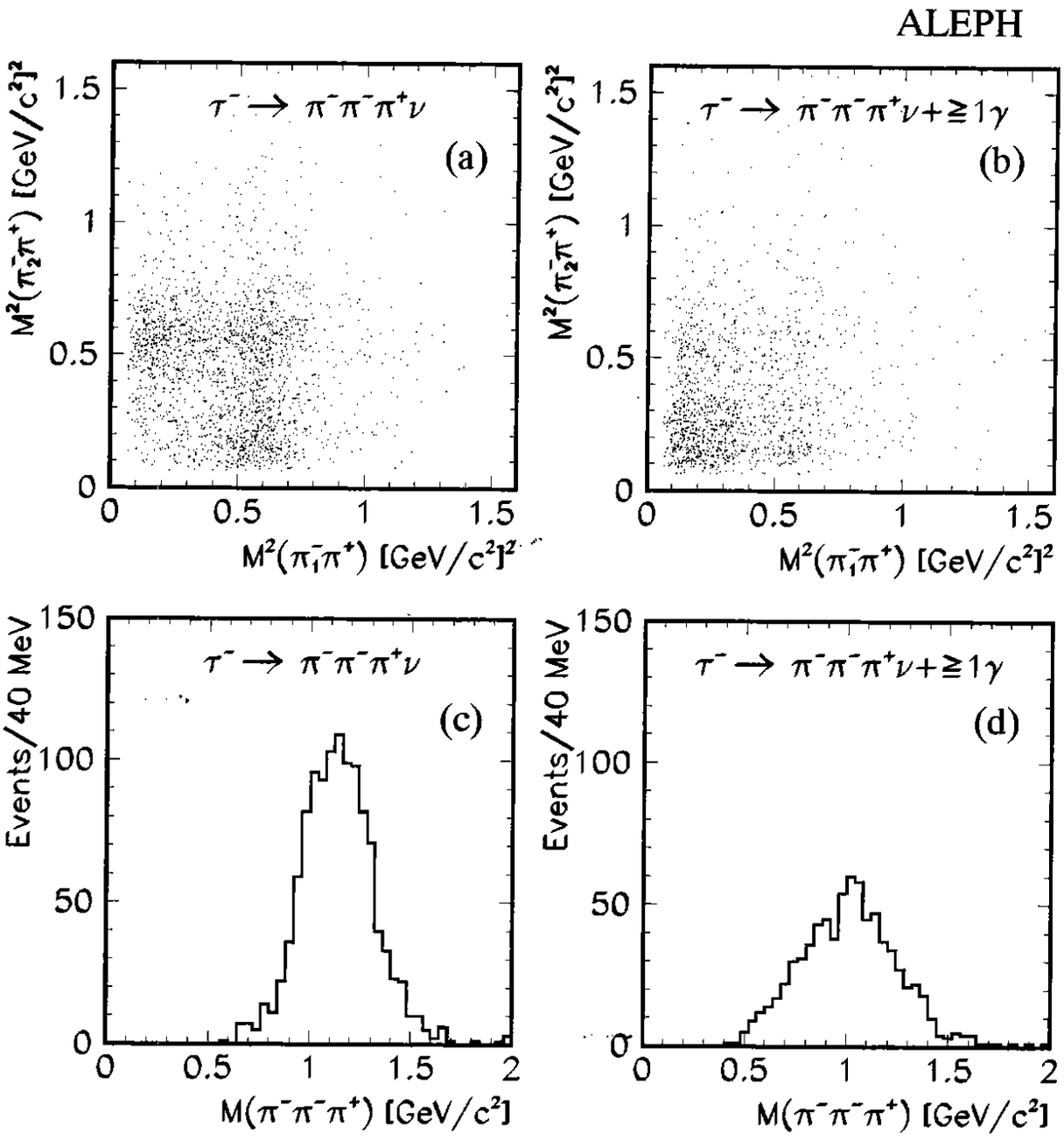
ALEPH
$\tau^- \to \pi^-\pi^-\pi^+\nu$
(a)
$\tau^- \to \pi^-\pi^-\pi^+\nu + \geq 1\gamma$
(b)
$M^2(\pi_2^-\pi^+)$ [GeV/c^2]^2
$M^2(\pi_1^-\pi^+)$ [GeV/c^2]^2
Events/40 MeV
$M(\pi^-\pi^-\pi^+)$ [GeV/c^2]
(c)
(d)

Fig.7

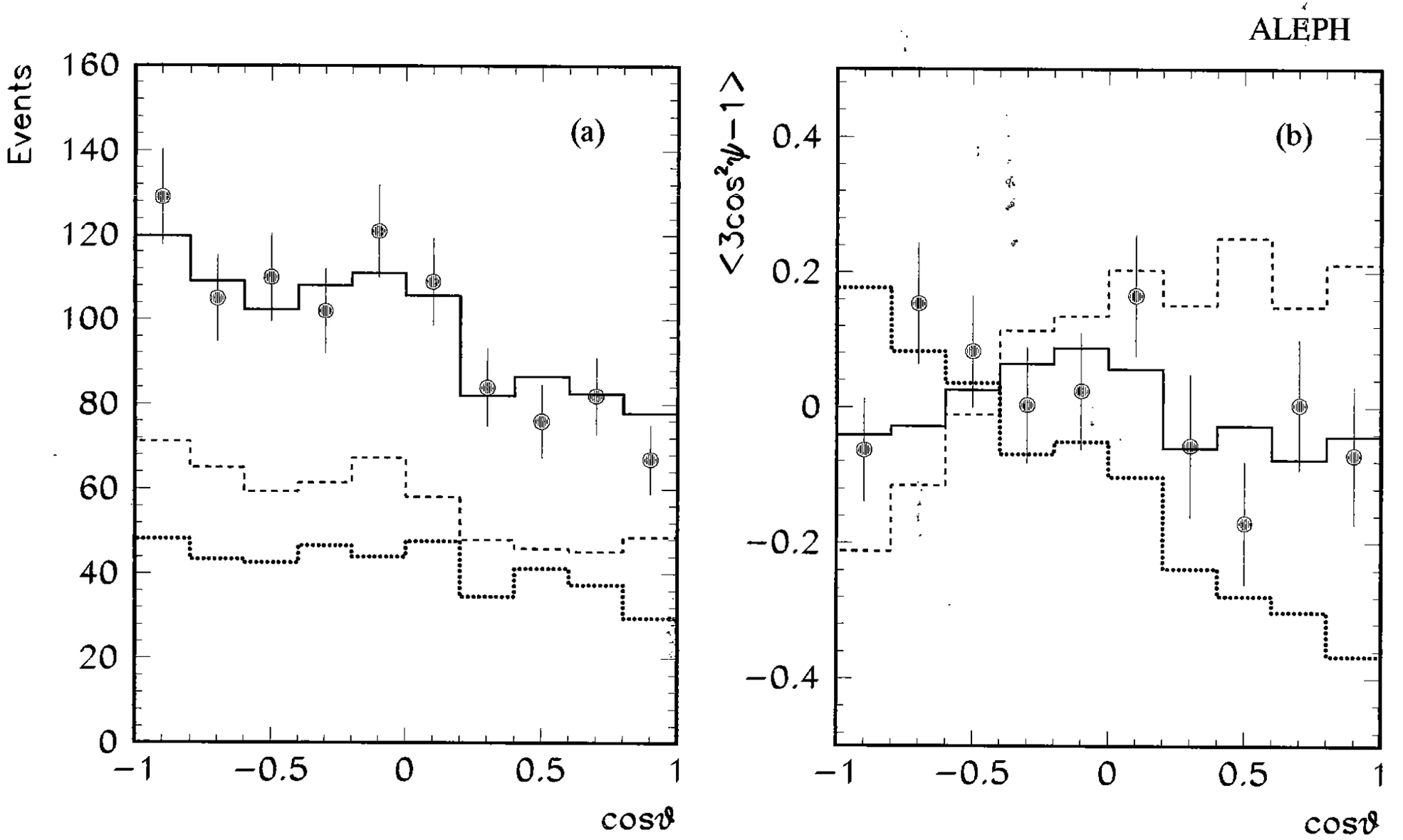
ALEPH
(a)
(b)
Events
$\langle 3\cos^2\psi - 1 \rangle$
cosϑ
cosϑ
160
140
120
100
80
60
40
20
0
0.4
0.2
0
−0.2
−0.4
−1
−0.5
0
0.5
1

Fig.8